Journal Pre-proof

Synchrotron Microbeam Radiotherapy for the treatment of lung carcinoma: a pre-clinical study

Verdiana Trappetti MSc , Cristian Fernandez-Palomo PhD , Lloyd Smyth PhD , Mitzi Klein VMD , David Haberthür PhD , Duncan Butler PhD , Micah Barnes MSc , Nahoko Shintani PhD , Michael de Veer PhD , Jean A. Laissue MD , Marie C. Vozenin PhD , Valentin Djonov MD

PII: S0360-3016(21)02630-4
DOI: https://doi.org/10.1016/j.ijrobp.2021.07.1717
Reference: ROB 27214

To appear in: *International Journal of Radiation Oncology, Biology, Physics*

Received date: 15 April 2021
Revised date: 7 July 2021
Accepted date: 30 July 2021

Please cite this article as: Verdiana Trappetti MSc , Cristian Fernandez-Palomo PhD , Lloyd Smyth PhD , Mitzi Klein VMD , David Haberthür PhD , Duncan Butler PhD , Micah Barnes MSc , Nahoko Shintani PhD , Michael de Veer PhD , Jean A. Laissue MD , Marie C. Vozenin PhD , Valentin Djonov MD , Synchrotron Microbeam Radiotherapy for the treatment of lung carcinoma: a pre-clinical study, *International Journal of Radiation Oncology, Biology, Physics* (2021), doi: https://doi.org/10.1016/j.ijrobp.2021.07.1717

Title: Synchrotron Microbeam Radiotherapy for the treatment of lung carcinoma: a pre-clinical study

Short Running Title: Synchrotron MRT for lung carcinoma

Author Names: Verdiana Trappetti MSc[1], Cristian Fernandez-Palomo PhD[1], Lloyd Smyth PhD[2], Mitzi Klein VMD[3], David Haberthür PhD[1], Duncan Butler PhD[3], Micah Barnes MSc[3,4], Nahoko Shintani PhD[1], Michael de Veer PhD[5], Jean A. Laissue MD[1], Marie C. Vozenin PhD[6], Valentin Djonov MD[1].

Author Institutions: 1- Institute of Anatomy, University of Bern, Switzerland; 2- Department of Obstetrics and Gynaecology, University of Melbourne, Royal Women's Hospital, Melbourne 3- Imaging and Medical Beamline, Australian Nuclear Science and Technology Organisation - Australian Synchrotron, Clayton, VIC, Australia; 4- Department of Physical Sciences, Peter MacCallum Cancer Centre, Melbourne, VIC, Australia; 5- Monash Biomedical Imaging, Monash University, Clayton, Australia; 6- Department of Radiation Oncology/CHUV, Lausanne University Hospital and University of Lausanne, Switzerland

Corresponding Author: Valentin Djonov, valentin.djonov@ana.unibe.ch

Author Responsible for Statistical Analysis: Valentin Djonov, valentin.djonov@ana.unibe.ch

Conflict of Interest Statement: Conflict of Interest: None

Funding Statement: We acknowledge financial support from the Australian Synchrotron, the Swiss National Foundation (31003A_176038), Swiss Cancer Research foundation (KFS-4281-08-2017) and the Bernische Krebsliga (Grant number 190).

Data Availability Statement for this Work: Research data are stored in an institutional repository and will be shared upon request to the corresponding author.

Acknowledgements: The authors wish to acknowledge Daniel Hausermann, Matthew Cameron and Clare Scott for experimental support on site at the Australian Synchrotron; Liam Day and Stefan Bartzsch for Monte Carlo modelling of the lung irradiation set-up; Helen Forrester for post-irradiation animal care and monitoring; the National Imaging Facility (NIF) and Monash Biomedical Imaging (MBI), Australia, for scientific and technical assistance; Tara Sepehrizadeh for technical support during the *in vivo* CT scans; Benoit Petit for assistance during the establishment of the tumour implantation method; Alexander Ernst for image analysis. Microscopy was performed on equipment supported by the Microscopy Imaging Center (MIC) of the University of Bern, Switzerland.

Abstract

Purpose - In the last three decades, Synchrotron Microbeam Radiation Therapy (S-MRT) has been shown to achieve both good tumour control and normal tissue sparing in a range of pre-clinical animal models. However, the use of S-MRT for the treatment of lung tumours has not yet been investigated. This study is the first to evaluate the therapeutic efficacy of S-MRT for the treatment of lung carcinoma, using a new syngeneic and orthotopic mouse model.

Methods and materials - Lewis Lung carcinoma-bearing mice were irradiated with two cross-fired arrays of S-MRT or Synchrotron Broad-Beam (S-BB) radiotherapy. S-MRT consisted of 17 microbeams with a width of 50 µm and centre-to-centre spacing of 400 µm. Each microbeam delivered a peak entrance dose of 400 Gy while S-BB delivered a homogeneous entrance dose of 5.16 Gy (corresponding to the S-MRT valley dose).

Results - Both treatments prolonged the survival of mice relative to the untreated controls (CTR). However, mice in the S-MRT group developed severe pulmonary oedema around the irradiated carcinomas and did not have improved survival relative to the S-BB group. Subsequent *post-mortem* examination of tumour size revealed that the mice in the S-MRT group had notably smaller tumour volume compared to the S-BB group, despite the presence of oedema. Mice that were sham-implanted did not display any decline in health following S-MRT, experiencing only mild and transient oedema between 4 days and 3 months post-irradiation which disappeared after 4 months. Finally, a parallel study investigating the lungs of healthy mice showed the complete absence of radiation-induced pulmonary fibrosis 6 months after S-MRT.

Conclusions - S-MRT is a promising tool for the treatment of lung carcinoma, reducing tumour size compared to mice treated with S-BB and sparing healthy lungs from pulmonary fibrosis. Future

experiments should focus on optimising S-MRT parameters to minimise pulmonary oedema and maximise the therapeutic ratio.

Keywords:

Synchrotron, Microbeams, Lung Carcinoma, Mouse

Introduction

Lung cancer is the deadliest type of cancer, responsible for 1.8 million deaths worldwide in 2020.[1] Radiotherapy is indicated for around three-quarters of all patients with lung cancer,[2] however, minimising acute and late radiation-induced side effects while controlling tumour growth remains a major challenge. Radiation-induced pneumonitis (RIP) is the most relevant acute toxic effect after conventional radiotherapy to the thorax,[3] while the most prominent long-term toxicity is radiation-induced pulmonary fibrosis (RIPF), which has an incidence of up to 28%.[4] RIPF is not only detrimental to quality-of-life, but can also lead to fatal respiratory insufficiency.[5]

Stereotactic Body Radiation Therapy (SBRT) is a cutting-edge radiotherapy approach for the treatment of early-stage non-small cell lung cancer (NSCLC) and is associated with excellent rates of local disease control.[6] However, SBRT can induce severe collateral effects including pneumonitis, rib fracture, and esophagitis, especially when treating centrally located lung tumours.[7] For this reason, SBRT is predominantly applied to small peripheral lesions.

Synchrotron Microbeam Radiation Therapy (S-MRT) is an innovative technique that employs the spatial fractionation of a synchrotron-generated X-ray beam into microbeams, typically between 20 and 100 µm wide. This geometry exploits dose-volume effect, where the tissue tolerance-dose increases as the proportion of irradiated tissue decreases.[8] Additionally, S-MRT utilises ultra-high dose-rates, most often providing the capability of delivering treatments in less than 200 ms[9] and thereby triggering a FLASH normal tissue sparing effect. This combination of the FLASH effect and spatial fractionation makes S-MRT a unique cancer treatment tool.

A vast body of pre-clinical research demonstrates that S-MRT effectively delays tumour growth or even ablates malignancies whilst being very well tolerated by normal tissue.[10] So far, S-MRT has been studied using a limited number of cancer types, most commonly *in vivo* models of brain tumours.[11,12] Mammary tumours,[13] melanoma,[14] and squamous cell carcinoma[15] have also been investigated. Mechanisms underlying the tumoricidal efficacy of S-MRT are (i) direct cellular radiation damage in the path of the microbeams,[16] (ii) selective disruption of immature vessels,[17] and (iii) enhancement of immune-cell recruitment.[14] Together with excellent tumour control, S-MRT shows pronounced tissue-sparing effects in several organs such as the skin,[18] central nervous system,[19] and mature vasculature.[20] Results from these studies are highly encouraging, but additional cancer types must be investigated to promote clinical translation.

The first S-MRT feasibility study for lung irradiation was recently published, demonstrating that the C57BL/6 mouse model is well suited to explore the potential of S-MRT for the treatment of lung cancer.[21] The lungs of healthy mice were irradiated with a peak S-MRT dose of 400 Gy or 40 Gy using microbeams with a width of 50 µm and a centre to centre spacing of 400 µm.[21] Moreover, preliminary

(unpublished) data from our group indicates that S-MRT causes only low-grade lung fibrosis in rats up to 12 months after irradiation. Given its superior tumour control and observed sparing of the normal lung, S-MRT could be a novel alternative for treating lung tumours, including central and ultra-central malignancies and cases where complete tumour resection is not possible.[22]

Here we show, for the first time, the successful application of S-MRT in a new pre-clinical mouse model of lung carcinoma. Tumour-bearing lungs were irradiated with either two cross-fired arrays of S-MRT or Synchrotron-Broad Beam (S-BB) radiation, with a control group receiving no treatment. In addition, S-MRT-induced changes in sham-injected lungs of healthy mice were observed with *in vivo* CT scans up to 6 months following irradiation. In parallel, the presence of fibrosis was also examined in S-MRT-irradiated lungs of naïve mice at the same time point.

Methods and Materials

Animals

Animal experimental procedures were performed under the XXXX license XXXX and the permits XXXX and XXXX approved by the XXXX Animal Ethics Committee. C57BL/6J female mice were purchased from the Animal Resources Centre (XXXX). Mice were 8 weeks old on arrival and were acclimatised for two weeks at the Medical beamline (XXXX) animal facility of the XXXX Synchrotron. Mice were housed at 23°C with a 12-hour light/12-hour dark cycle and had access to food and water *ad libitum*. For the survival study, animals were culled upon reaching interruption criteria. These criteria were assessed for each mouse on a daily basis using a score sheet. A composite score was calculated based on the domains of weight loss, overall appearance, passive behaviour and behaviour after stimulation. Severe

loss of weight (more than 15% from the day of irradiation), evident breathing problems, no reaction after stimulation, or a radiological tumour volume greater than 100 mm^3 based on *in vivo* CT, were criteria for immediate euthanasia.

Cell line

The murine Lewis Lung carcinoma (LLC1, also known as LL/2) cell line was purchased from the American Type Culture Collection (ATCC® CRL-1642™). Cells were cultured in Dulbecco's Modified Eagle's Medium (DMEM) supplemented with 10% (v/v) Foetal Bovine Serum (FBS) and kept at 37°C in a humidified incubator with 5% CO_2. Lewis Lung carcinoma is a type of NSCLC and KRAS-mutated tumour.[23] This cell line is clinically relevant because NSCLC accounts for 85% of all lung cancers[24] and KRAS –mutations are the most common in patients with lung adenocarcinoma.[25] It was chosen because it was originally derived from C57BL/6 mice lungs and therefore allowed the development of a syngeneic and orthotopic mouse model, immunologically compatible with the organism.[26] Cells were utilised before the seventh passage. On the day of tumour implantation, cells were detached from the flasks with a Trypsin solution (0.25%) and counted with a disposable Haemocytometer C-Chip (Model: DHC-N01, NanoEntek Inc., Seoul, South Korea). Cells were finally re-suspended in FBS-free DMEM at a concentration of 1 x 10^4 LLC1 cells per 3 µl.

LLC1 inoculations

The protocol for tumour inoculation was adapted from Mordant and colleagues.[27] Paracetamol in drinking water (2 mg/ml) was given 48 hours prior to implantation. Each mouse was weighed and anaesthetised with an intraperitoneal (IP) injection of an anaesthetic cocktail comprising of Fentanyl (0.05 mg/kg of body weight (BW)), Midazolam (5 mg/kg BW) and Medetomidine (0.5 mg/kg BW) in

sterile water. The body temperature of each mouse was maintained at 37°C during the whole procedure. Each mouse was laid on its left side exposing its right flank. The area of implantation (under the right-scapular region) was shaved with a trimmer and disinfected with a Chlorhexidine solution (2%). To provide local anaesthesia, a solution of Lidocaine (0.5%) was injected subcutaneously (SC) at the site of inoculation. To identify the injection site, a superficial imaginary line (subsequently referred to as the mid-axillary line), was drawn along the mid-sagittal plane. A skin incision of approximately 5 mm was made with surgical scissors along the mid-axillary line and the cutaneous maximus and latissimus dorsi muscles were gently separated to visualise the rib cage. LLC1 cells were injected with a Hamilton syringe between the third and the fourth rib. A 3 µl volume of cell culture medium containing 1 x 10^4 cells was supplemented with 2 µl of Thrombin solution (18 U/ml) immediately before the injection. The total injection volume was 5 µl. After the inoculation, the incision was closed with two interrupted sutures using a 6/0 polyamide monofilament non-absorbable surgical suture. A solution of Buprenorphine (0.1 mg/kg BW) was injected SC on the right flank to provide systemic analgesia. Anaesthesia was reversed with an IP injection of Flumazenil (0.5 mg/kg BW) and Atipamezole (2.5 mg/kg BW) in sterile water. Two mice were sham-injected: the animals underwent the whole surgical procedure but received an injection with no tumour cells.

Irradiation set-up

Irradiations were performed 11 days after LLC1 inoculations in Hutch 2B on the XXXX at the XXXX Synchrotron. After induction of anaesthesia (same protocol as used for the LLC1 inoculations), mice were orally intubated with a modified catheter under fibre optic guidance (Kent Scientific, Torrington, CT). Mice were then fixed with surgical tape onto a Perspex positioning frame and transferred onto the DynamicMRT small-animal irradiation stage.[28,29] A Physiosuite (Kent Scientific) ventilator/monitor

calculated the tidal volume and respiratory rate from the weight of the mouse. Mice were aligned to the synchrotron beam using an established image guidance system.[29] Deep inspiration breath-hold was employed for both imaging and irradiation to ensure correct alignment of the lung tumours to the beam. Mice were irradiated with either two cross-fired S-MRT arrays (13 mice) or two cross-fired S-BB fields (13 mice). Breath-hold, image guidance and irradiation were controlled from outside the irradiation hutch. S-MRT and S-BB were delivered using two anterior-oblique fields, centred on the tumour and separated by an angle of 25°. This angle was chosen to spare the spinal cord and the heart of the mouse. Mice were then disconnected from the ventilator, removed from the Perspex frame and given an IP injection of reversal cocktail (same as used for the tumour inoculations). Thirteen carcinoma-bearing mice were used as a non-irradiated control group (CTR). In addition, 14 healthy mice were irradiated with two cross-fired S-MRT arrays; six mice were culled 12 hours post-irradiation to verify that the microbeams were delivered correctly to the tumour via γH2AX staining and eight mice were culled 6 months post-irradiation to evaluate lung fibrosis. A further two sham-injected mice underwent periodic *in vivo* CT imaging to evaluate changes in the lungs up to 6 months post-irradiation.

Dosimetry

S-MRT and S-BB were delivered during operation at 3 GeV and with a ring current of 200 mA. The doses delivered to the tumour for both modalities were determined from Monte Carlo simulations using a phantom representative of the mouse and the plastic holder used for the irradiations. The mouse was modelled as a rectangular prism (100 mm long x 30 mm wide x 15 mm deep) composed of water, lying on a plastic plate (200 mm long, 150 mm wide, 5 mm deep) composed of poly-methyl-methacrylate. Mice were scanned vertically through a 2 mm high beam-slice using the DynamicMRT stage to deliver the prescribed doses to a total field size of 7 mm x 7 mm. Reference dosimetry was performed with a

PTW (Freiburg, Germany) Pinpoint 31014 ionisation chamber under broad-beam conditions at both the S-MRT and S-BB energy spectrums. For S-MRT (average energy 93 keV) each field delivered a peak entrance dose of 400 Gy (valley entrance dose = 2.86 Gy), equating to a peak and valley dose to the tumour (depth of 8.5 mm) of 353.6 Gy and 4.76 Gy, respectively. Each S-MRT field consisted of 17 microbeams of 50 µm width with 400 µm centre-to-centre spacing. The in-slice peak MRT dose-rate was 991.7 Gy/s at tumour depth (in-slice delivery time of 361 ms). The vertical scan speed of the mouse through the beam was 5.63 mm/s, leading to a total delivery time of 1.24 seconds for the entire field. For S-BB (average energy 124 keV), each field delivered an entrance dose of 5.16 Gy and a dose to the tumour of 4.76 Gy. The in-slice S-BB dose-rate was 37.0 Gy/s at 8.5 mm depth (in-slice delivery time of 129 ms) and the vertical scan speed was 15.63 mm/s. The total time to deliver the prescribed dose to the entire field was 447 ms. The uncertainties (k=1) associated with the delivered doses to the tumour were 4.1%, 3.9% and 8.5% for S-MRT (peak), S-MRT (valley) and S-BB, respectively.

The S-MRT valley dose matched the S-BB dose delivered to the tumour in order to distinguish the advantage of high peak doses in conjunction with those of homogenous radiation.

In vivo CT scans

In vivo lung CT scans were performed using a Siemens Inveon multi-modality scanner at the XXXX Biomedical Imaging facility (XXXX, XXXX). Scans were performed in step-and-shoot mode with 360 projections at 80 kV and 500 µA with a 180 ms exposure for each projection for a total scan time of 5 minutes. The image field-of-view was 38.63 x 33.64 mm with an effective pixel size of 40 µm. Animals were anaesthetised with isoflurane (2-2.5%) in 100% oxygen throughout the scan.

Tumour growth curve

The tumour growth curve for the LLC1 carcinoma model was obtained by measuring the tumour size from the *in vivo* CT scan images. Measurements were taken at day 8 and day 12 post-implantation and every third day thereafter. The maximum dimensions of the tumour in the sagittal, coronal, and transverse planes were recorded. Tumour volume (in mm^3) was calculated with the formula:

$$V = \frac{4}{3}\pi \times \frac{a}{2} \times \frac{b}{2} \times \frac{c}{2}$$

where a, b, and c are the maximum recorded lengths of the tumour in the sagittal, coronal, and transverse planes, respectively. Tumour doubling times were calculated between days 8-12, 12-15, 15-18 and day 18-21 post-implantation. Tumour doubling time was calculated with the formula:

$$Doubling\ time = (t_2 - t_1) \cdot \frac{\ln(2)}{\ln\left(\frac{V_2}{V_1}\right)}$$

where V_2 and V_1 are the tumour volumes at the later (t_2) and earlier (t_1) time points, respectively.

Survival curves

Kaplan-Meier survival curves were generated and analysed using Prism version 9.0.1 (GraphPad Software, San Diego, CA).

Post-mortem micro-CT scans

Mice were euthanised with an IP injection of Sodium Pentobarbital (200mg/kg BW) and lungs were fixed with 4% PFA post-mortem. Fixation was followed by either critical point drying in the case of the model characterization study or paraffin embedding for the lungs coming from the survival study. Samples were imaged on a Bruker SkyScan 1272 high-resolution micro-tomography machine (Bruker micro-CT, Kontich, Belgium). The X-ray source was set to a tube voltage of 50.0 kV and a tube current of 200.0 µA, the x-ray spectrum was not filtered prior to incidence onto the sample. A set of 962 projections of 2452 x 1640 pixels were recorded every 0.2° over a 180° rotation for each sample. Every individual projection was exposed for 273 ms and 5 projections were averaged to reduce image noise. This resulted in scan times of approximately 55 minutes and an isometric voxel size of 8.0 µm in the final data sets. The projection images were subsequently reconstructed into a 3D stack of images with NRecon version 1.7.4.2 (Bruker microCT, Kontich, Belgium). Lung carcinomas were manually segmented from the 3D stack and their volumes were calculated with Imaris image version 9.3 (Bitplane, Zürich, Switzerland).

Immunohistochemistry

Mice lungs were instilled with a 2% paraformaldehyde solution through a *post-mortem* tracheotomy.[21] The harvested lungs were fixed in 4% paraformaldehyde for 24 hours, dehydrated in ethanol and finally embedded in paraffin. Immunohistochemistry was performed on 5 µm thick paraffin sections of the

lungs using rabbit polyclonal antibodies against pan Cytokeratin (Bioss Antibodies, Woburn, MA), CD31 (Abcam, Cambridge, UK) and rabbit monoclonal antibody against Ki67 (Clone SP6) (ThermoFisher Scientific, Fremont, CA). Deparaffinised sections underwent antigen retrieval using Tris-EDTA buffer (pH 9) for CD31, EDTA buffer (pH 8) for pan Cytokeratin and citrate buffer (pH 6) for Ki67. After a blocking step (3% skimmed bovine milk with 2.5% goat serum), the sections were incubated with the primary antibody (1 hour at 37°C). Endogenous peroxidase activity was blocked with 0.6% hydrogen peroxide in methanol. ImmPRESS® goat anti-rabbit IgG (Vector Laboratories, Burlingame, CA) was used to detect the primary antibodies binding to CD31, pan Cytokeratin, and Ki67. For CD31 and pan Cytokeratin, the Biotin-Free Tyramide Signal Amplication System (DAKO, Carpinteria, CA) was used. The sections were stained with NovaRed (Vector Laboratories) and cell nuclei were counterstained with haematoxylin. Stained sections were evaluated and photographed in an IMAGER.M2 light microscope (Carl Zeiss Microscopy GmbH, Jena, Germany).

Quantification of Ki67 nuclear immunoreactivity

To quantify Ki67 nuclear immunoreactivity of tumour cells, the sections stained with anti-Ki67 antibody were analysed. Two to 4 different areas per section were chosen using a 20x objective. The images obtained were analysed with ImageJFiji software,[30] version 2.0.0-rc-69/1.52p. One or two regions of interest (ROIs) per image were defined so that each ROI contained at least 200 to 400 tumour cells. ROIs were defined within 500 µm from the edge of the tumour. Ki67 positive and negative tumour cells in each ROI were manually counted using the ImageJ Plugin Cell counter.[31] Ki67 immunoreactivity was expressed as a percentage of positive cells over the total number of tumour cells analysed. Data were analysed with Prism version 9.0.1 (GraphPad Software).

Immunofluorescence

Twelve hours following S-MRT, normal mouse lungs were harvested, fixed in PFA and embedded in paraffin as described above. After deparaffinisation (protocol described above), the tissue sections underwent antigen retrieval (citrate buffer, pH 6). Sections were then incubated with 2% BSA/PBS/0.3% Triton for 15 minutes and a second blocking solution (4.5 ml PBS-Triton 0.3%, 0.5 ml donkey serum, 0.15 g milk powder) for 1 hour at room temperature. Sections were incubated overnight at 4°C with the primary Ab, rabbit anti-gamma H2A.X-phospho S139 (Abcam) in blocking solution. On the morning of the following day, sections were incubated with a donkey anti-rabbit Alexa Fluor488 secondary antibody (Life Technologies, Carlsbad, CA), and DAPI in blocking solution for 6 hours at 4°C. Images were acquired with a Zeiss LSM 880 confocal microscope (Carl Zeiss Microscopy GmbH, Jena, Germany).

Quantification of lung fibrosis

The lungs of irradiated normal mice were harvested 6 months following S-MRT irradiation, fixed in 4% PFA, and embedded in paraffin as described above. Five sets of paraffin-embedded lungs were randomly selected for processing and analysis. The lungs were cut coronally from caudal to cranial. Then, 5 µm thick sections were obtained from five different locations separated by 200 µm throughout the tissue. Only the most caudal portion of the remaining 3 lungs were examined. Sections were deparaffinised and stained with Masson-Goldner trichrome.[32,33] Lung fibrosis was scored in all sections according to the method described by Hübner et al.[34] Grade 0 corresponds to the absence of any fibrotic alteration in the lungs. Grade 1 to 8 describe progressive lung fibrosis where Grade 1 indicates minimal fibrosis and Grade 8 total fibrosis with destruction of the lung structure.

Results

The LLC1 model

The tumour growth curve for the LLC1 model is shown in Fig. 1A. Tumour doubling times were 1.62 days, 1.89 days, 2.55 days and 4.19 days for the intervals between day 8-12, 12-15, 15-18 and 18-21 post-irradiation, respectively. Reconstructed 3D images from *post-mortem* micro-CT scans of the whole lungs at 11 (Fig. 1B) and 14 (Fig. 1C) days post-irradiation showed solid tumours localised in the caudal lobe of the right lung. The choice of controlled tumour placement by injection over a spontaneous tumour model allowed for tumour development at a sufficient distance from the central airways and the heart.

Pan-cytokeratin staining at all time points (11, 14 and 17 days post-implantation) revealed a well circumscribed tumour with well-defined pushing borders, but not surrounded by a fibrous capsule isolating it from the adjacent lung tissue (Fig. 2A-C). Staining for the CD31 protein (also known as PECAM-1), a marker for endothelial cells of blood vessels, showed the tumours were well vascularised with regularly distributed intra-tumoural micro-vessels (Fig. 2D-F). Tumours stained for the Ki67 nuclear protein showed a homogenous proliferative pattern at all the evaluated time points (Fig. 2G-I). The ratio of proliferating cells, calculated as the percentage of Ki67 positive cells over the total number of carcinoma cells within the tumour slice, was statistically significant between day 11 and day 17 post-implantation (p=0.0419) and increased over time (Fig. S2).

Dosimetry and irradiation set-up

A schematic representation of the irradiation set-up is shown in Fig. 3A. Gafchromic EBT-XD films (Ashland, Bridgewater, NJ) confirmed the microbeam configuration (50 µm beam width and 400 µm on-centre spacing) as well as the angle of 25° between the two cross-fired S-MRT arrays (Fig. 3B) and S-BB fields (Fig. 3C). Immunofluorescent γH2AX staining for DNA damage on lung slices corroborated the correct delivery of the two cross-fired S-MRT arrays through the whole right lung at 12 hours post-irradiation (Fig. 3D). The same staining was performed in S-BB irradiated lung slices (Fig. 3E). A table summarizing dosimetry parameters is reported in Fig. 3F.

Survival

Kaplan-Meier Survival curves (Fig. 4A) demonstrated that both S-MRT and S-BB significantly increased the survival of the carcinoma-bearing mice relative to the CTR group. There were no statistically significant differences in survival between the S-BB and S-MRT groups (p=0.3173). Median survival times were 7, 11 and 12 days for the control, S-BB and S-MRT groups, respectively (Fig. 4B).

Radiological evaluation of LLC1 carcinomas with *in vivo* CT imaging

In vivo CT imaging of mice from the CTR group confirmed the presence of a well-defined pulmonary mass, identified as the LLC1 carcinoma, in the right lung from 3 days prior to irradiation to day 10 post-irradiation (Fig. 5A). The increased contrast and defined borders of the pulmonary mass allowed for precise measurements of the tumour volume. This was also the case for mice in the S-BB treated group (Fig. 5B). However, the CT images of mice belonging to the S-MRT group started to show fluid opacity surrounding the carcinomas from day 4 post-irradiation, which became evident on days 7 and 10 (Fig.

5C). The radiological finding of fluid opacity is attributable to pulmonary oedema. The presence of oedema hindered the identification of the tumour borders and the ability to measure tumour size for the S-MRT group. Finally, RIP cannot be excluded from the CT imaging of the S-MRT group.

Post-mortem evaluation of tumour size with micro-CT imaging and histological analysis

Lungs from the same mice shown in Fig. 5A-C were harvested at 10 days post-irradiation after reaching the experimental endpoints. *Post-mortem* perfusion to remove blood and dehydration (post-fixation) of the lungs allowed for visualisation of the tumour mass only, using micro-CT imaging, without the oedema (Fig. 5D-F). These images clearly demonstrated that the LLC1 carcinomas subjected to S-MRT were the smallest of the three groups. The calculated post-segmentation volumes for these carcinomas were 45.49 mm^3, 24.5 mm^3 and 3.04 mm^3 for the CTR, S-BB and S-MRT groups, respectively. Histological examination with haematoxylin and eosin confirmed the reduced tumour size in the S-MRT group compared to S-BB and CTR tumours (Fig. 5D-F).The proliferation ratio at this time point (10 days post-irradiation) also appeared lower for the S-MRT treated tumour compared to the S-BB irradiated and non-irradiated tumours (Fig. S3), however, this difference was not statistically significant.

The observation of a smaller size for the S-MRT treated tumour was also made in mice sacrificed upon reaching experimental endpoints at day 7 (CTR) and day 8 (S-BB and S-MRT) following irradiation. Macroscopic pictures and histological evaluation (via haematoxylin and eosin staining) confirmed that the size of the tumour receiving S-MRT was clearly smaller compared to those receiving S-BB or no irradiation (Fig. S4).

Evaluation of long-term side effects with CT imaging

In vivo CT images for the sham-implanted and S-MRT irradiated mice, from scans taken periodically over the course of 6 months, are shown in Fig. 6. An opacity attributable to a moderate form of liquid effusion was observed from day 4 up to 3 months post-irradiation (Fig. 6C-F). However, this opacity was no longer detectable four months post-irradiation (Fig. 6G). No health impairments were detected in either of these mice throughout the six-month follow-up period.

Evaluation of long-term fibrosis

In the 8 healthy mice subjected to S-MRT, staining of lung sections with Masson-Goldner trichrome at 6 months post-irradiation revealed a score 0 on the Hübner scale for all samples, corresponding to the absence of fibrotic changes (Fig. 6I).

Discussion

Previous S-MRT research demonstrates amelioration of survival and exceptional tumour control in pre-clinical models of glioma, melanoma, and mammary carcinoma[10]. The present study adds to this body of research by showing, for the first time, the efficacy of S-MRT for the treatment of lung carcinoma. Although we did not demonstrate a significant increase in survival time after S-MRT relative to S-BB (Fig. 4), port-mortem analysis found that S-MRT was the most effective modality for reducing tumour size (Fig. 5D-F and Fig. S4). However, because this was designed as a survival study, there was an insufficient number of samples harvested at pre-established time points to confirm whether this observation was statistically significant. For this purpose, future mechanistic studies should be performed.

A further key finding of this study was the development of oedema, and possible acute RIP around the tumours, following S-MRT (Fig. 5). The detrimental effects of pulmonary oedema on respiratory function and overall well-being is likely to be the reason why there was no survival advantage for the S-MRT group compared to the S-BB group. In contrast, serial *in vivo* CT scans of the sham-implanted mice showed only a minor and transient form of liquid effusion following S-MRT. A similar observation of mild, transient oedema was made previously in a study of normal rat brains irradiated with doses up to 1000 Gy by an S-MRT array of 25 µm wide microbeams with a centre-to-centre spacing of 211 µm.[35] Taken together, these observations suggest that the presence of the malignancy itself was a critical contributor to the extent of the observed pulmonary oedema in the S-MRT group. It has been demonstrated that the vascular toxicity and consequent vascular disruption caused by S-MRT depends on the stage of vessel maturation.[17, 20] Tumours have immature vasculature, and therefore would be more susceptible to significant tumour capillary disruption and pulmonary oedema following S-MRT.

Importantly, the present study also demonstrated that S-MRT did not cause long-term lung fibrosis, even after delivering a high total peak dose (400 Gy x 2 = 800 Gy). This suggests that there may be a potential benefit for patients who require aggressive radiation treatment that might otherwise significantly deteriorate their long-term quality of life. Future experiments should aim to prevent the formation of oedema while maintaining the demonstrated tumour control and long-term absence of fibrosis. The concomitant administration of S-MRT with other strategies known to reduce pulmonary oedema should be considered, including supplemental oxygen or pharmacological treatment with Glyceryl trinitrate or furosemide.[36] In addition, careful selection of S-MRT delivery parameters, such as peak dose, microbeam width and spacing, dose-rate and temporal fractionation, may also be crucial for the success of S-MRT for treating lung carcinoma.

A peak-dose of 400 Gy was chosen for this study based on the demonstrated therapeutic efficacy of this S-MRT dose for several other pre-clinical cancer models.[10] However, for these previous studies, a smaller microbeam centre-to-centre spacing of 200 µm was used.[10] To compensate for the use of a 400 µm centre-to-centre microbeam spacing – the only available configuration at the XXXX Synchrotron – we chose to cross-fire two S-MRT arrays, each delivering 400 Gy, for a total peak dose of 800 Gy peak to the tumour and adjacent areas of surrounding normal lung tissue. In retrospect, this very high total dose may have exceeded the structural tolerance of the lung tissue, contributing to the observed pulmonary oedema. For future experiments, the total peak-dose could be reduced and the use of multiple cross-fired S-MRT arrays avoided, if a smaller centre-to-centre spacing between the microbeams is used.

Increasing the S-MRT dose-rate further may also contribute to diminishing the acute oedema observed in the tumour-bearing mice. There is evidence that the FLASH normal tissue sparing effect is proportional to the applied dose-rate.[37,38] Therefore, using a dose-rate even higher than 991.7 Gy/s (in-slice delivery time of 361 ms for S-MRT) could help to reduce, or even prevent, the basal fluid effusion from normal lung tissue which was observed in the sham-implanted mice and could have contributed to the pulmonary oedema in the tumour-bearing mice. Increasing the dose-rate, in combination with employing a narrower collimator and a reduced total peak dose, could help to balance effective vascular disruption in the tumor with sparing of the surrounding normal lung tissue. Repeating these experiments at the XXXX Synchrotron Radiation Facility (XXXX), where dose-rates of up to 16000 Gy/s can be employed, will allow for an evaluation of the contribution of dose-rate amplitude to the prevention of acute pulmonary oedema following S-MRT.

Finally, an additional strategy that should be adopted in future experiments is temporal fractionation of the total S-MRT dose. A recent study showed that fractionating the dose with respect to time by administering S-MRT as three consecutive daily doses of 133 Gy resulted in a 50% rate of complete tumour remission in a mouse model of melanoma.[39] This approach is likely to favour the therapeutic efficacy of S-MRT on lung cancer by also reducing the risk of pulmonary oedema.

For future *in vivo* studies, S-MRT parameters should be carefully determined by considering the sensitivity of the treated organ bearing the malignancy. For the treatment of lung carcinoma we propose the use of a microbeam centre-to-centre spacing of 200 µm, a total peak dose of 400 Gy administered daily over two to three consecutive days (e.g. 2 x 200 Gy or 3 x 133 Gy), and an ultra-high dose-rate in the order of 1 x 10^4 Gy/s. These considerations aim to reduce collateral effects – particularly pulmonary oedema in lung cancer models – and may increase the therapeutic effect of S-MRT in the treatment of other unexplored tumours types.

Conclusions

In the present study, we have made a significant step towards using S-MRT for the treatment of lung cancer by successfully targeting and treating a localised lung carcinoma in a pre-clinical model. We have demonstrated that S-MRT increases survival compared to non-irradiated controls and reduces the size of tumours whilst not causing fibrotic changes up to six months post-irradiation. Optimising S-MRT parameters to reduce the risk of pulmonary oedema will maximize its therapeutic potential and clinical translation for the treatment of lung malignancies.

References

1. Cancer. https://www.who.int/news-room/fact-sheets/detail/cancer.
2. Delaney, G., Barton, M., Jacob, S. & Jalaludin, B. A model for decision making for the use of radiotherapy in lung cancer. *Lancet Oncol.* **4**, 120–128 (2003).
3. Keffer, S., Guy, C. L. & Weiss, E. Fatal Radiation Pneumonitis: Literature Review and Case Series. *Adv. Radiat. Oncol.* **5**, 238–249 (2019).
4. Chen, Z., Wu, Z. & Ning, W. Advances in Molecular Mechanisms and Treatment of Radiation-Induced Pulmonary Fibrosis. *Transl. Oncol.* **12**, 162–169 (2018).
5. Ding, N.-H., Li, J. J. & Sun, L.-Q. Molecular Mechanisms and Treatment of Radiation-Induced Lung Fibrosis. *Curr. Drug Targets* **14**, 1247–1356 (2013).
6. Tsang, M. W. K. Stereotactic body radiotherapy: current strategies and future development. *J. Thorac. Dis.* **8**, S517–S527 (2016).
7. Thompson, M. & Rosenzweig, K. E. The evolving toxicity profile of SBRT for lung cancer. *Transl. Lung Cancer Res.* **8**, 48–57 (2019).
8. Zeman, W., Curtis, H. J. & Baker, C. P. Histopathologic Effect of High-Energy-Particle Microbeams on the Visual Cortex of the Mouse Brain. *Radiat. Res.* **15**, 496–514 (1961).
9. Bourhis, J. *et al.* Clinical translation of FLASH radiotherapy: Why and how? *Radiother. Oncol.* **139**, 11–17 (2019).
10. Fernandez-Palomo, C. *et al.* Animal Models in Microbeam Radiation Therapy: A Scoping Review. *Cancers* **12**, (2020).
11. Bouchet, A. *et al.* Permeability of Brain Tumor Vessels Induced by Uniform or Spatially Microfractionated Synchrotron Radiation Therapies. *Int. J. Radiat. Oncol. Biol. Phys.* **98**, 1174–1182 (2017).
12. Serduc, R. *et al.* Synchrotron microbeam radiation therapy for rat brain tumor palliation-influence of the microbeam width at constant valley dose. *Phys. Med. Biol.* **54**, 6711–6724 (2009).
13. Crosbie, J. C. *et al.* Tumor cell response to synchrotron microbeam radiation therapy differs markedly from cells in normal tissues. *Int. J. Radiat. Oncol. Biol. Phys.* **77**, 886–894 (2010).
14. Potez, M. *et al.* Synchrotron Microbeam Radiation Therapy as a New Approach for the Treatment of Radioresistant Melanoma: Potential Underlying Mechanisms. *Int. J. Radiat. Oncol. Biol. Phys.* **105**, 1126–1136 (2019).
15. Miura, M. *et al.* Radiosurgical palliation of aggressive murine SCCVII squamous cell carcinomas using synchrotron-generated X-ray microbeams. *Br. J. Radiol.* **79**, 71–75 (2006).
16. Fernandez-Palomo, C. *et al.* γ-H2AX as a Marker for Dose Deposition in the Brain of Wistar Rats after Synchrotron Microbeam Radiation. *PLOS ONE* **10**, e0119924 (2015).
17. Brönnimann, D. *et al.* Synchrotron microbeam irradiation induces neutrophil infiltration, thrombocyte attachment and selective vascular damage in vivo. *Sci. Rep.* **6**, 33601 (2016).
18. Potez, M. *et al.* Effects of Synchrotron X-Ray Micro-beam Irradiation on Normal Mouse Ear Pinnae. *Int. J. Radiat. Oncol. Biol. Phys.* **101**, 680–689 (2018).

19. Laissue, J. A. *et al.* Neuropathology of ablation of rat gliosarcomas and contiguous brain tissues using a microplanar beam of synchrotron-wiggler-generated X rays. *Int. J. Cancer* **78**, 654–660 (1998).
20. Sabatasso, S. *et al.* Microbeam Radiation-Induced Tissue Damage Depends on the Stage of Vascular Maturation. *Int. J. Radiat. Oncol. Biol. Phys.* **80**, 1522–1532 (2011).
21. Schültke, E. *et al.* A Mouse Model for Microbeam Radiation Therapy of the Lung. *Int. J. Radiat. Oncol.* (2020) doi:10.1016/j.ijrobp.2020.12.030.
22. Sharma, V. J. *et al.* Low recurrence of lung adenoid cystic carcinoma with radiotherapy and resection. *ANZ J. Surg.* **89**, 1051–1055 (2019).
23. Agalioti, T. *et al.* Mutant KRAS promotes malignant pleural effusion formation. *Nat. Commun.* **8**, 15205 (2017).
24. Oser, M. G., Niederst, M. J., Sequist, L. V. & Engelman, J. A. Transformation from non-small-cell lung cancer to small-cell lung cancer: molecular drivers and cells of origin. *Lancet Oncol.* **16**, e165-172 (2015).
25. Ghimessy, A. *et al.* Current therapy of KRAS-mutant lung cancer. *Cancer Metastasis Rev.* **39**, 1159–1177 (2020).
26. Kellar, A., Egan, C. & Morris, D. Preclinical Murine Models for Lung Cancer: Clinical Trial Applications. *BioMed Res. Int.* **2015**, e621324 (2015).
27. Mordant, P. *et al.* Bioluminescent orthotopic mouse models of human localized non-small cell lung cancer: feasibility and identification of circulating tumour cells. *PloS One* **6**, e26073 (2011).
28. Livingstone, J. *et al.* Preclinical radiotherapy at the Australian Synchrotron's Imaging and Medical Beamline: instrumentation, dosimetry and a small-animal feasibility study. *J. Synchrotron Radiat.* **24**, 854–865 (2017).
29. A patient-positioning system for synchrotron micro-beam radiotherapy (MRT) - RMIT University. https://researchrepository.rmit.edu.au/esploro/outputs/graduate/A-patient-positioning-system-for-synchrotron-micro-beam-radiotherapy-MRT/9921863984801341.
30. Schindelin, J. *et al.* Fiji: an open-source platform for biological-image analysis. *Nat. Methods* **9**, 676–682 (2012).
31. Cell Counter. *ImageJ* https://imagej.net/Cell_Counter?
32. MASSON, P. Some histological methods : Trichrome staining and their preliminary technique. *J Tech Methods* **12**, 75–90 (1929).
33. Goldner, J. A modification of the masson trichrome technique for routine laboratory purposes. *Am. J. Pathol.* **14**, 237–243 (1938).
34. Hübner, R.-H. *et al.* Standardized quantification of pulmonary fibrosis in histological samples. *BioTechniques* **44**, 507–511, 514–517 (2008).
35. Serduc, R. *et al.* Characterization and quantification of cerebral edema induced by synchrotron x-ray microbeam radiation therapy. *Phys. Med. Biol.* **53**, 1153–1166 (2008).
36. Purvey, M. & Allen, G. Managing acute pulmonary oedema. *Aust. Prescr.* **40**, 59–63 (2017).
37. Montay-Gruel, P. *et al.* Irradiation in a flash: Unique sparing of memory in mice after whole brain irradiation with dose rates above 100Gy/s. *Radiother. Oncol.* **124**, 365–369 (2017).
38. Wilson, J. D., Hammond, E. M., Higgins, G. S. & Petersson, K. Ultra-High Dose Rate (FLASH) Radiotherapy: Silver Bullet or Fool's Gold? *Front. Oncol.* **9**, (2020).

39. Fernandez-Palomo, C. *et al.* Complete Remission of Mouse Melanoma after Temporally Fractionated Microbeam Radiotherapy. *Cancers* **12**, (2020).

Figure captions

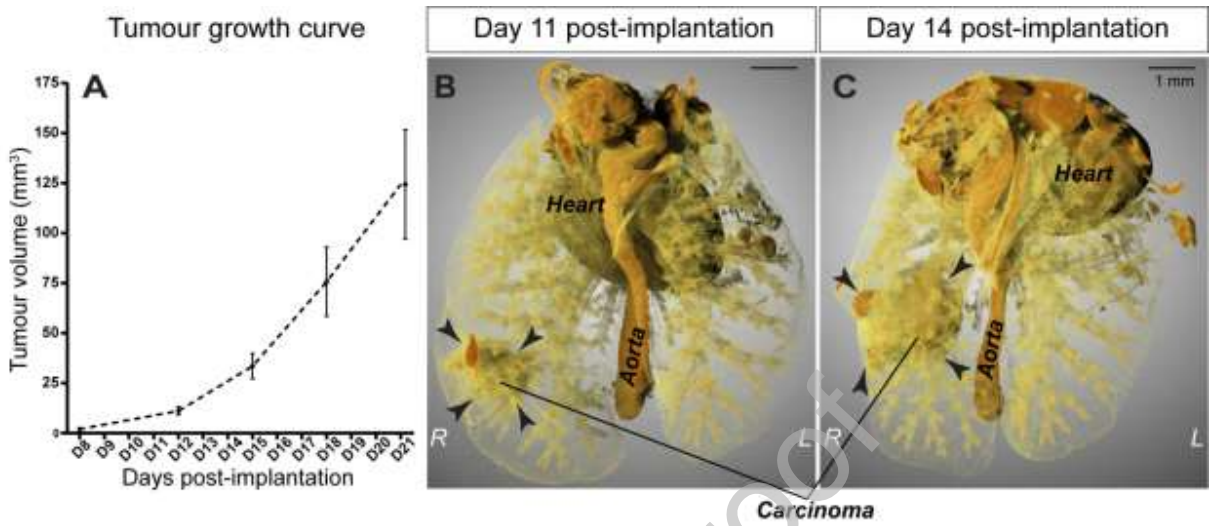

Fig. 1 – *LLC1 tumour model growth dynamics.* (A) LLC1 tumour growth curve in the absence of treatment. 3D reconstructed *post-mortem* micro-CT images of the lungs of tumour-bearing mice at 11 (B) and 14 days post-implantation (C). The ventral view is shown. Black arrows indicate the carcinomas.

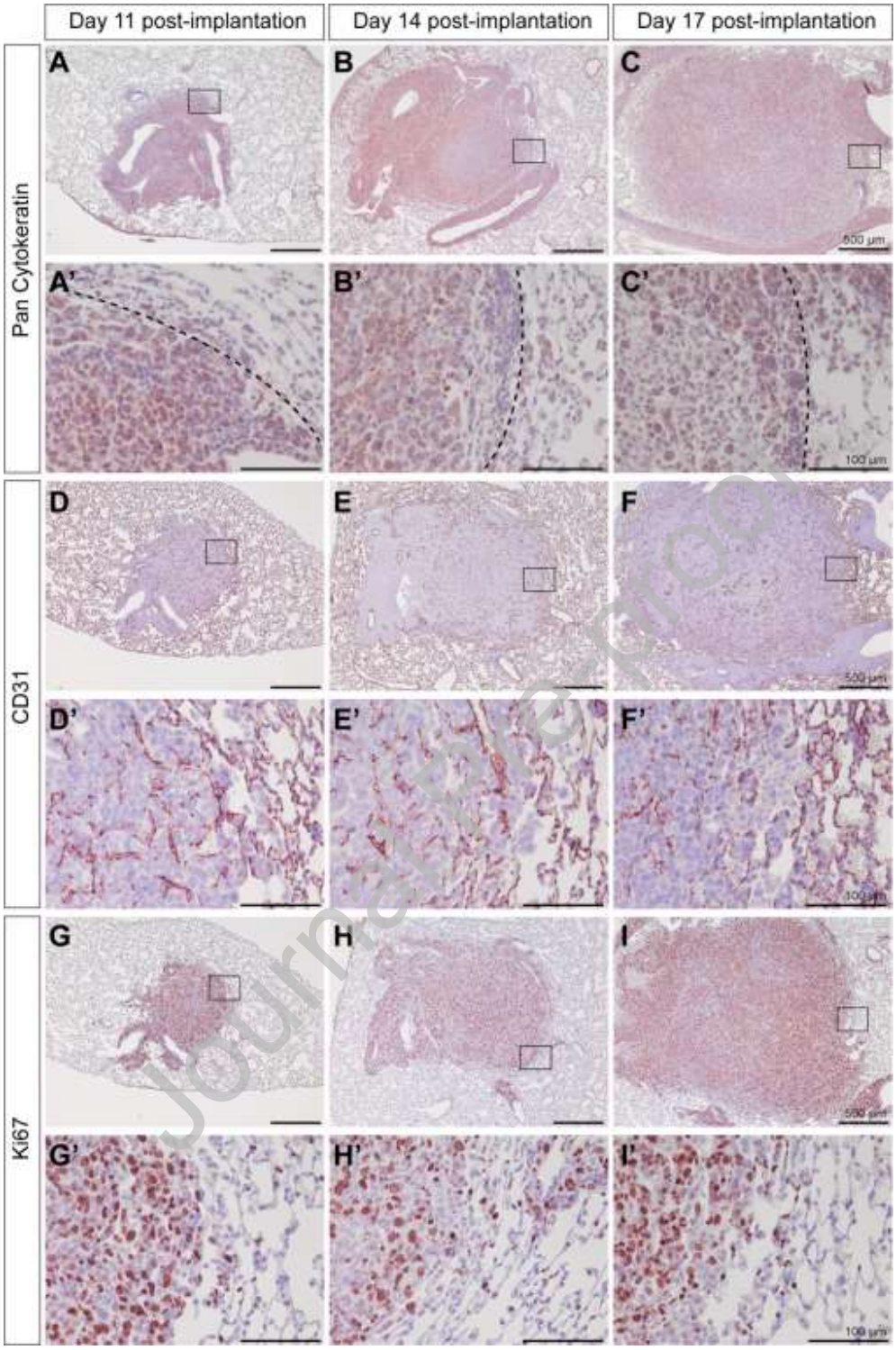

Fig. 2 – *Histological characterisation of the LLC1 tumour model.* Pan Cytokeratin staining (NovaRed) showed clear localisation of the carcinomas in the lung tissue at 11 (A), 14 (B), and 17 (C) days post-

implantation. Higher magnification images of pan Cytokeratin staining revealed the tumour borders (dotted line in A', B' and C'). Images of tumours stained for CD31 (NovaRed) showed well-vascularised tumours with regular blood vessel distribution at 11 (D, D'), 14 (E, E') and 17 days post-implantation (F, F'). Images for Ki67 staining (NovaRed) demonstrated persistent proliferative activity at 11 (G, G'), 14 (H, H') and 17 days post-implantation (I, I').

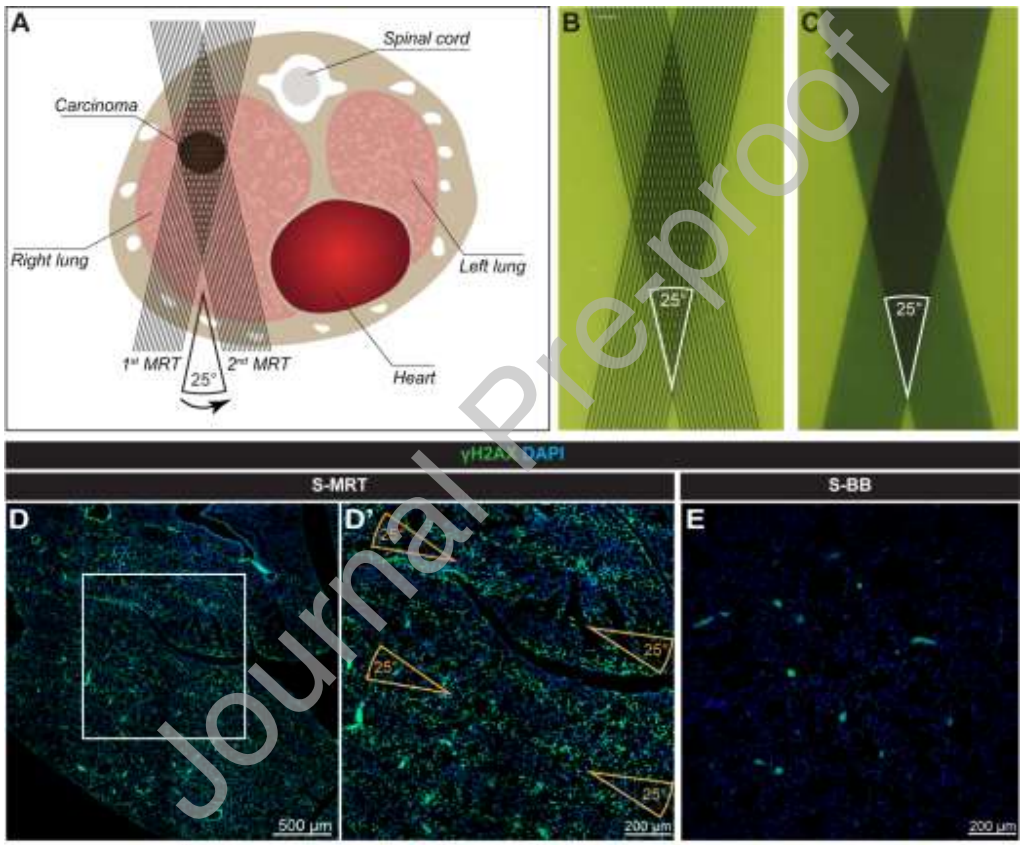

F

	Entrance dose	Dose at tumour	Valley entrance dose	Valley dose at tumour	Dose-rate	In-slice delivery time	Total delivery time
S-MRT	400 Gy peak	353.6 Gy peak	2.86 Gy	4.76 Gy	991.7 Gy/s	361 ms	1.24 s
S-BB	5.16 Gy	4.76 Gy	–	–	37.0 Gy/s	129 ms	447 ms

Fig. 3 – *S-MRT irradiation set-up.* (A) Schematic representation of the mouse thorax (axial view) with the two cross-fired S-MRT arrays targeting the tumour. Gafchromic films confirmed the geometry of the two

microbeams arrays (B) and of the S-BB fields (C). (D, D') Immunofluorescent staining for γH2AX (positive green nuclei) in irradiated normal lungs harvested at 12 hours post-irradiation verified the successful delivery of the two cross-fired S-MRT arrays to the right lung. (E) The same staining at 12 hours post-treatment confirmed the S-BB delivery. (F) Table summarizing dosimetry parameters.

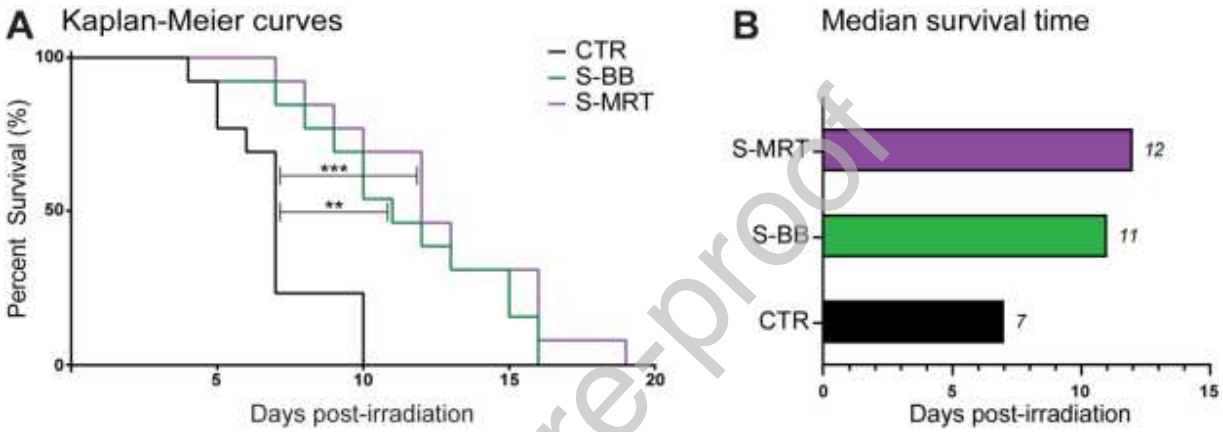

Fig. 4 – *Post-irradiation survival.* (A) Kaplan-Meier survival curves and (B) median survival times for the control (CTR, black), S-BB (green) and S-MRT (purple) groups. The Log-rank (Mantel-Cox) test showed that the differences in survival between CTR vs S-BB (** p=0.0014) and CTR vs S-MRT (**** p<0.0001) were statistically significant. The difference in survival between S-BB vs S-MRT was not statistically significant.

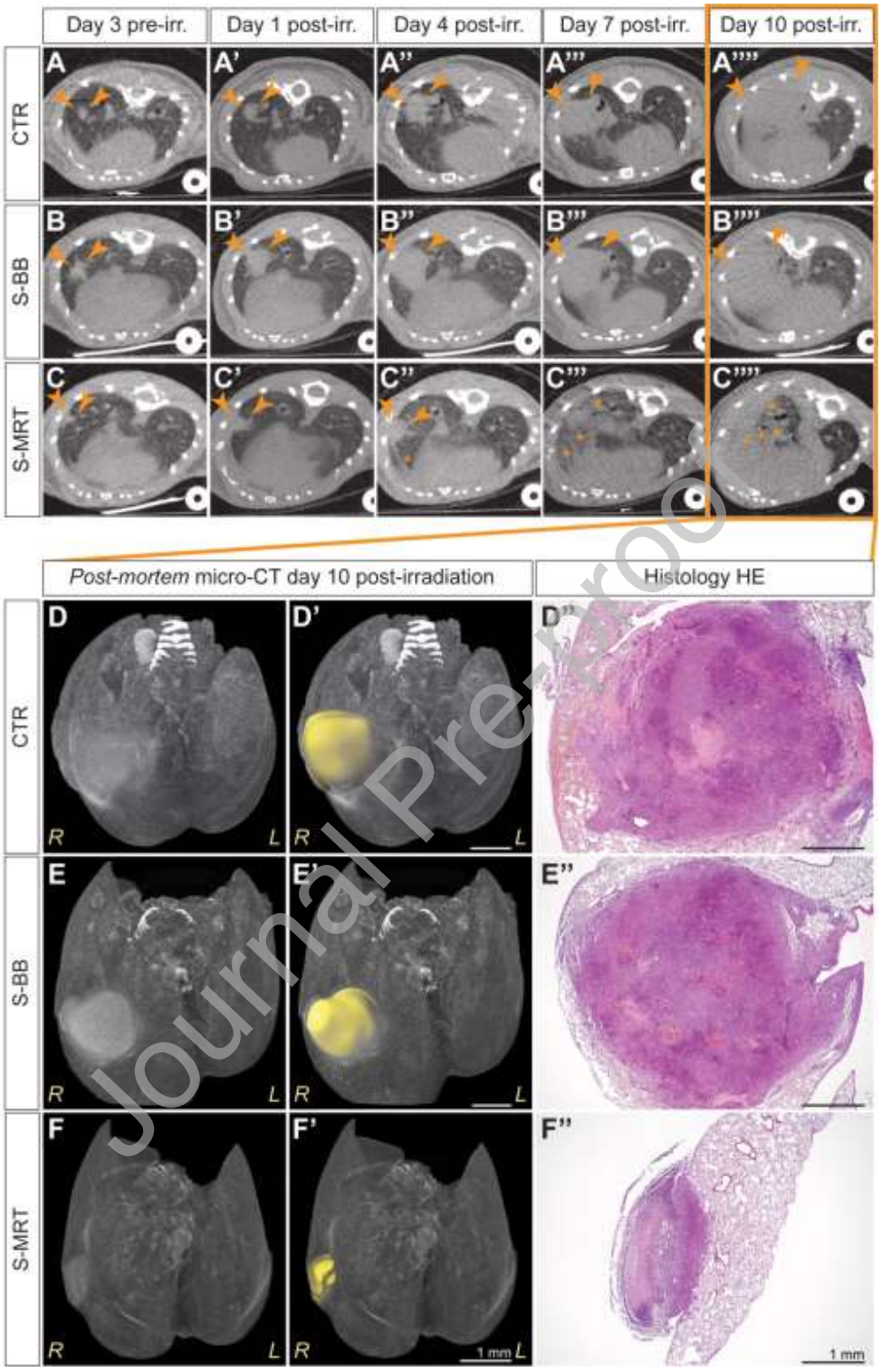

Fig. 5 – *Monitoring of tumour development. In vivo* CT imaging of carcinomas three days prior to irradiation and 1, 4, 7 and 10 days post-irradiation for tumours in CTR (panels A to A''''), S-BB (panels B

to B'''') and S-MRT (panels C to C’’’’) groups. Extensive pulmonary oedema was observed only in the S-MRT group (asterisks, panel C’’ to C’’’’). The tumours depicted by the *in vivo* CT images at 10 days post-irradiation were subsequently evaluated by *post-mortem* micro-CT and manually segmented; CTR (D, D’), S-BB (E, E’), S-MRT (F, F’). Histological evaluation (haematoxylin and eosin staining) of the same tumours is shown in panel D’’ (CTR), E’’ (S-BB) and F’’ (S-MRT). Histology and *post-mortem* micro-CT revealed substantially smaller lesions for S-MRT compared to both S-BB and CTR groups at 10 days post-irradiation.

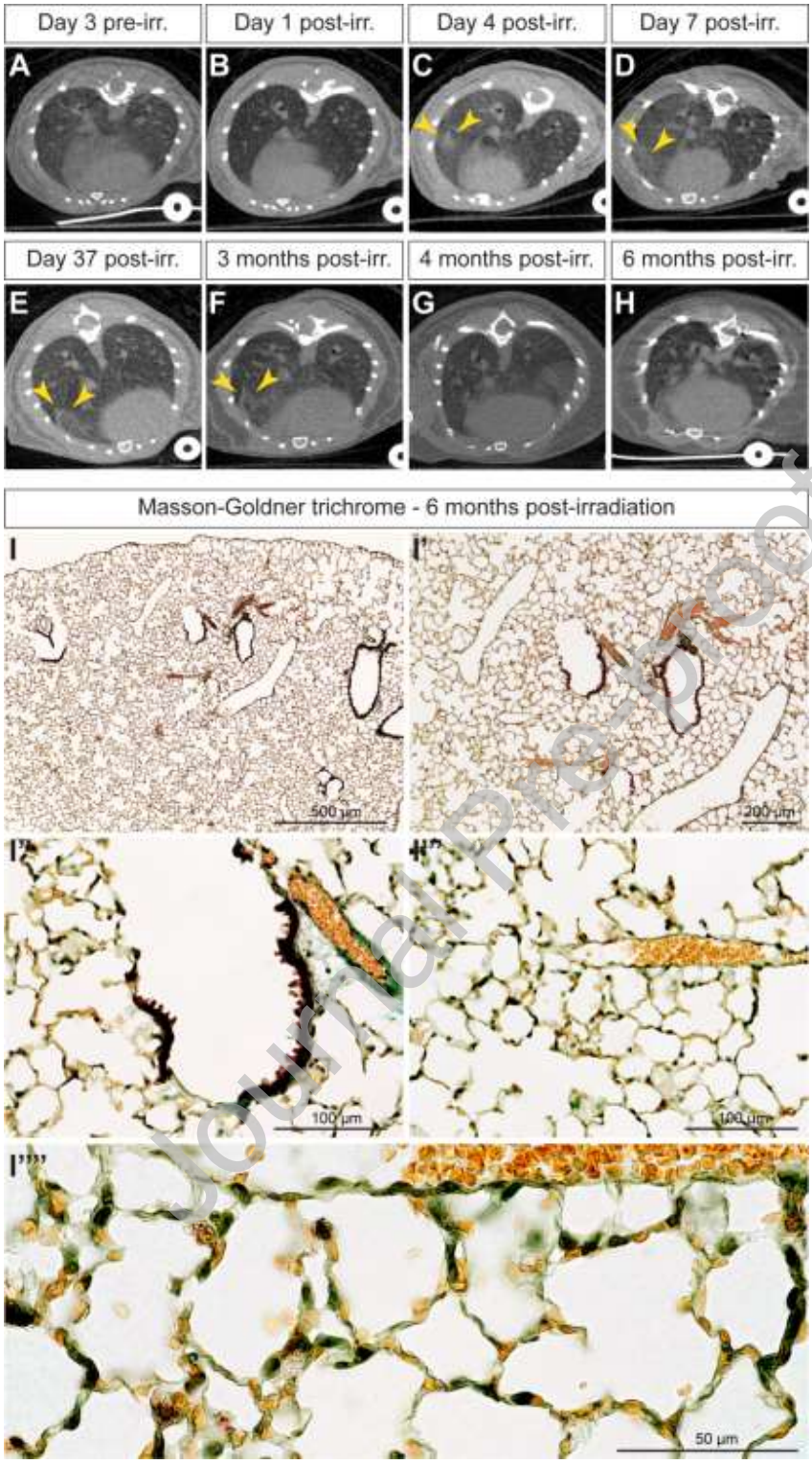

Fig. 6 – *Long-term study of healthy lungs following irradiation.* Sham-implanted mice which received S-MRT were evaluated over 6 months by *in vivo* CT scans. Scans were performed 3 days prior to irradiation

(A), then at day 1 (B), day 4 (C), day 7 (D), day 37 (E), 3 months (F), 4 months (G) and 6 months (H) post-irradiation. Fluid opacity is indicated with yellow arrowheads in C, D, E and F. (I to I’’’’) Masson-Goldner trichrome stained lung sections at increasing magnification demonstrate no evidence of lung fibrosis at 6 months post-irradiation. Panel I’’’’ is part of I’’’. Panels I’’’ and I’’ are parts of I’, that is part of I.